Ultrafast Charge Carrier Recombination and Trapping in Hematite Photoanodes under Applied Bias

Stephanie R Pendlebury,*,† Xiuli Wang,† Florian Le Formal,† Maurin Cornuz,‡ Andreas Kafizas,† S. David Tilley,‡ Michael Grätzel,‡ and James R Durrant*,†

†Department of Chemistry, Imperial College London, South Kensington Campus, London, SW7 2AZ, United Kingdom

‡Institut des Sciences et Ingénierie Chimiques, Ecole Polytechnique Fédérale de Lausanne, Laboratory of Photonics and Interfaces, Station 6, CH-1015 Lausanne, Switzerland

ⓈSupportingInformation

ABSTRACT: Transient absorption spectroscopy on subpicosecond to second time scales is used to investigate photogenerated charge carrier recombination in Si-doped nanostructured hematite (α-Fe_2O_3) photoanodes as a function of applied bias. For unbiased hematite, this recombination exhibits a 50% decay time of ~6 ps, ~10^3 times faster than that of TiO_2 under comparable conditions. Anodic bias significantly retards hematite recombination dynamics, and causes the appearance of electron trapping on ps–μs time scales. These ultrafast recombination dynamics, their retardation by applied bias, and the associated electron trapping are discussed in terms of their implications for efficient water oxidation.

Metal oxide semiconductors, such as hematite (α-Fe_2O_3), TiO_2, and $BiVO_4$, are of interest for solar-driven fuels synthesis (artificial photosynthesis) due to their ability to oxidize water, stability, and variable nanomorphology. Photoelectrochemical (PEC) water oxidation on such metal oxide photoanodes exhibits rate constants in the range 10^{-2} to 1 s^{-1},[1–4] requiring the generation of long-lived holes with lifetimes of milliseconds to seconds. The generation of such long-lived holes is limited by electron/hole recombination processes, which have been reported on time scales ranging from subpicoseconds to seconds.[1,5–7] The generation of a space charge layer (SCL) at the semiconductor surface under anodic bias has been shown to retard such recombination losses; however, such studies have been limited to date to microsecond to second time scales. Previous ultrafast spectroscopic studies have resolved substantial subnanosecond electron/hole recombination in some metal oxides. Indeed for hematite,[6,8–13] some studies have reported almost complete recombination within a few hundreds of picoseconds, 10^8 times faster than the rate constant for water oxidation, and in striking contrast to the high quantum efficiencies for PEC water oxidation reported under continuous irradiation at anodic (positive) bias.[14,15] This apparent discrepancy may in part be related to the relatively high carrier densities sometimes generated in ultrafast spectroscopy, which can accelerate recombination rates. More significantly, there are no published reports of the effect of applied electrical bias (voltage) on recombination on ultrafast (sub-100 ps) time scales. Since efficient water oxidation on metal oxide photoanodes occurs only under anodic applied bias, knowledge of the effect of bias on the charge carrier dynamics is vital to understanding the efficiency limitations of such solar energy conversion systems.

Herein we compare the charge carrier dynamics in nanostructured Si-doped hematite[16] with those of nanocrystalline anatase TiO_2.[17] We show for the first time that ps–ns electron/hole recombination in hematite is significantly retarded by positive bias. These studies also indicate that, in hematite under anodic bias, electron trapping competes with ultrafast electron/hole recombination. We suggest this may aid the generation of long-lived holes at the semiconductor surface. The implications of these results are discussed with respect to the efficiency of solar water splitting.

Our previous studies employed transient absorption spectroscopy (TAS) to investigate charge carrier dynamics on microsecond to second time scales in hematite and anatase TiO_2 photoanodes in a photoelectrochemical cell.[1,2,7] The yield of long-lived (ms–s) holes was observed to correlate with the photocurrent density as a function of applied electrical bias. Thus, applied bias is expected to have a significant effect on sub-ms trapping and recombination kinetics, which limit the yield of long-lived holes and hence O_2 evolution.

Typical transient absorption kinetics for nanostructured Si-doped hematite (APCVD α-Fe_2O_3) and nanocrystalline anatase (n-TiO_2) on femto- to nanosecond time scales in an inert atmosphere (i.e., in the absence of applied bias) are shown in Figure 1 (spectra are shown in Figures S2 and S3). For both oxides, a broad photoinduced absorption is observed (500–800 nm), with hematite spectra exhibiting a clear maximum at 575 nm. These spectra are in agreement with previous reports[5,6,12,18,19] and are assigned to the absorption of photogenerated charges. Figure 1 shows the decay dynamics of these broad absorption signals at a representative probe wavelength (750 nm) as a function of excitation density. The transient absorption signal for n-TiO_2 is initially approximately constant and then decays on the 100 ps–ns time scale. In contrast, the hematite transient kinetics exhibit a markedly faster decay, which begins within the time resolution of the measurements (ca. 200 fs). Similar decay kinetics were observed for all probe wavelengths studied, in an inert atmosphere (Figures S3 and S4). The decay half-times ($t_{50\%}$)
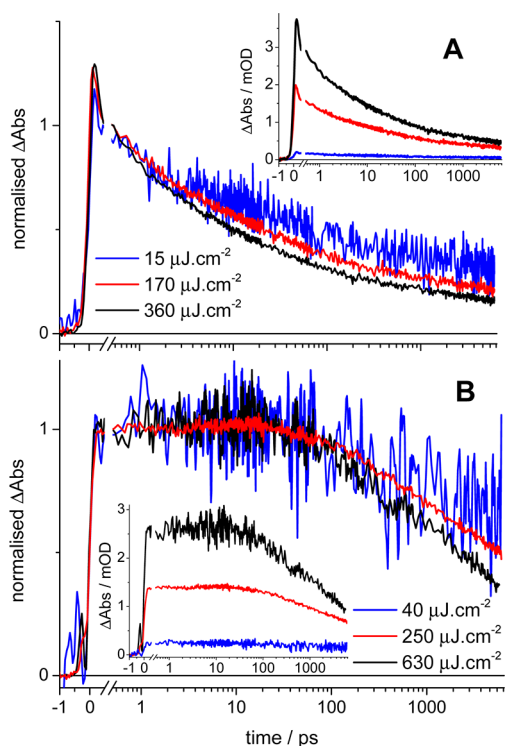
Figure 1. Transient absorption kinetic decays probed at 750 nm under nitrogen, normalized at 0.5 ps, as a function of excitation intensity (355 nm, 500 Hz; excitation intensities are per laser pulse; non-normalized decays inset). (A) Si-doped nanostructured α-Fe$_2$O$_3$ (2.4 $\times$ 10^{13}−5.8 $\times$ 10^{14} photons absorbed·cm^{-2}·pulse^{-1}). (B) Nanocrystal-line TiO$_2$ (6.7 $\times$ 10^{13}−5.2 $\times$ 10^{14} photons absorbed·cm^{-2}·pulse^{-1}).

for α-Fe$_2$O$_3$ and n-TiO$_2$ are 3 ps and 6.2 ns, respectively, under similar excitation density conditions (black lines in Figure 1 A and B). Analogous fast transient absorption decays have been widely reported for hematite.[6,8−13]

The decay kinetics of both n-TiO$_2$ and α-Fe$_2$O$_3$ are retarded with decreasing excitation density (e.g., $t_{50\%}$ for hematite increases from 3 to 20 ps for 360 to 15 μJ·cm^{-2}·pulse^{-1}, respectively), indicative of bimolecular recombination of separated charges (i.e., nongeminate electron/hole recombination). Consistent with this assignment, these decay dynamics partially fit to power law decays, $\Delta OD \propto t^{\alpha}$, with $\alpha \sim$0.15 for these α-Fe$_2$O$_3$ photoanodes (Figure S5). These results are indicative of dispersive recombination in the presence of significant disorder or charge trapping.[20] For all excitation densities examined, the hematite decay dynamics were 100−1000 times faster than those for titania. Faster dynamics for hematite relative to titania were also observed for a range of films, including doped and undoped hematite, and nanocrystalline and dense titania (Figure S6). While the detailed origin of this difference in dynamics between hematite and titania is beyond the scope of this communication, it is clear that avoiding ultrafast electron/hole recombination is a particular challenge for PEC water oxidation by hematite photoanodes. This challenge is the focus for the remainder of this communication.

Figure 1 demonstrates that unbiased hematite photoanodes exhibit substantial ultrafast, bimolecular recombination. We now consider the extent to which applied anodic bias can reduce this recombination. The effect of applied electrical bias on the transient absorption spectra and decay kinetics of hematite photoanodes in a PEC cell is shown in Figure 2 (the corresponding photocurrent data are shown in Figure S7). The kinetics and spectra of α-Fe$_2$O$_3$ in electrolyte (0.1 M NaOH) with no applied electrical bias (Figure S8) are similar to those at $\sim$0.9 V$_{RHE}$, just cathodic of the photocurrent onset and in agreement with the open circuit potential. It is evident from Figure 2 that applied electrical bias strongly affects the charge carrier dynamics, even on picosecond time scales.

The evolution of the ps−ns transient absorption spectra with applied electrical bias is shown in Figure 2 A and B. Under flat-
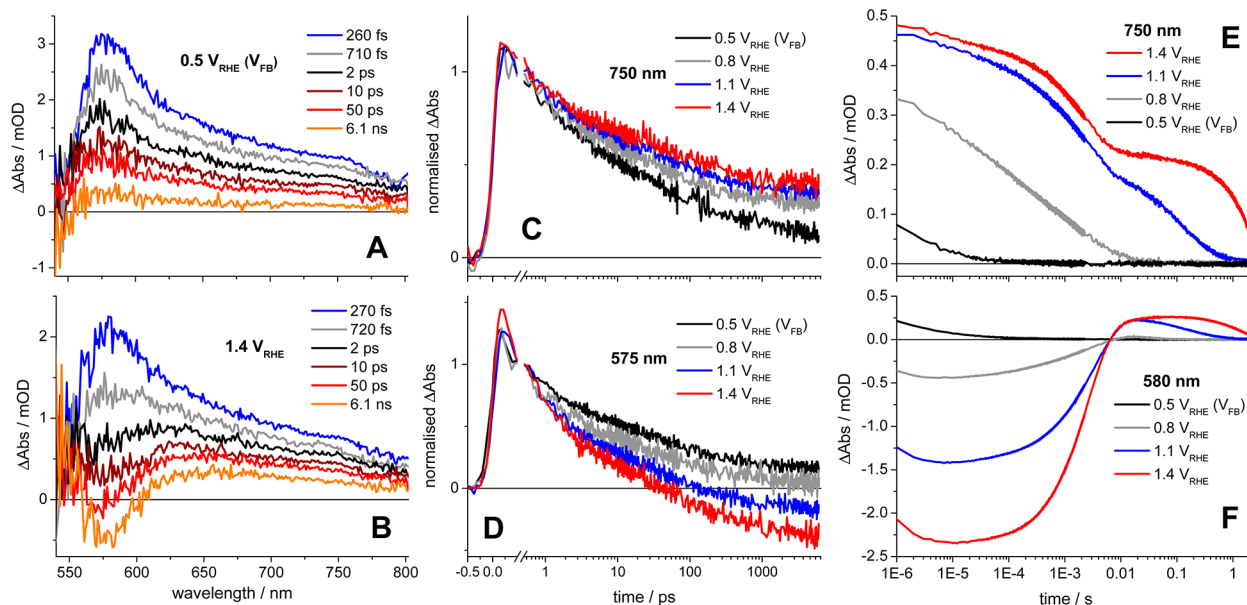

Figure 2. fs−ns transient absorption spectra of Si-doped APCVD hematite under applied bias (A, B), and kinetics (normalized at 0.5 ps) probed at 750 nm (C) and 575 nm (D) (355 nm, 500 Hz, 110 μJ·cm^{-2}·pulse^{-1}). Corresponding TA kinetics on μs−s time scales (355 nm, 0.33 Hz, 200 μJ·cm^{-2}·pulse^{-1}) (E, F). Electrolyte−electrode (EE) excitation of hematite working electrode in a three-electrode cell (Pt gauze counter and Ag|AgCl| sat. KCl reference electrodes) with 0.1 M NaOH electrolyte (pH 12.8).

band conditions ($\sim$0.5 V_{RHE},[21] V_{FB}) a broad positive absorption is observed, peaking at 570−580 nm, which decays to a small residual positive signal over the time range studied (up to 6 ns). This decay under flatband conditions is assigned, as above, primarily to bimolecular recombination of photogenerated electrons and holes. At 1.4 V_{RHE}, anodic of the photocurrent onset (Figure S7), a similar initial broad, positive photoinduced absorption is observed. However, the temporal evolution of this photoinduced absorption is substantially different from that observed under flat-band conditions. For wavelengths >625 nm, anodic bias is observed to result in a significant retardation of the decay kinetics on the time scale studied (200 fs−6 ns). In contrast, under anodic bias the initial positive absorption maximum at $\sim$575 nm rapidly inverts to a negative (bleach) signal. Our previous μs−s-TAS and spectroelectrochemical studies have indicated that the broad absorption observed on microsecond to second time scales for wavelengths >625 nm can be assigned to hematite hole absorption, while the negative (bleach) signal observed at $\sim$575 nm under anodic bias can be assigned to electron trapping by localized states located close to the conduction band edge.[2,16] Figure 2C and 2D show ultrafast transient kinetics illustrative of these two spectral regions, at 750 and 575 nm. Figure 2E and 2F plot the corresponding transient kinetics on microsecond to second time scales. It is apparent that these slower time scale data, which are analogous to those we have reported previously,[22] are in good agreement with the ultrafast data shown in Figure 2A−D.

We first consider the transient kinetics at 750 nm, assigned primarily to photoinduced absorption of hematite holes.[22] At 0.5 V_{RHE} (flat-band potential), where there is expected to be no space-charge field to aid electron/hole separation, this transient signal exhibits a rapid dispersive power-law decay from subpicosecond to microsecond time scales, with $t_{50\%}$ $\sim$6 ps. As in the absence of applied bias, this decay is assigned to bimolecular electron/hole recombination. The application of positive bias results in a substantial retardation of decay kinetics at this wavelength on all time scales studied (ps−s). For example, at 1.4 V_{RHE}, $t_{50\%}$ increases to $\sim$200 ps, resulting in extension of the signal to the seconds time scale. It is possible that a small contribution to the ultrafast signal decay at this wavelength may be associated with a loss of photoinduced electron absorption, due to electron trapping (discussed below) and recombination.[6] Therefore, we are unable to quantify ultrafast recombination losses. Nevertheless, these data provide, to the best of our knowledge, the first direct evidence that anodic bias is indeed capable of substantially increasing ultrafast charge carrier lifetimes in a metal oxide photoanode. This is attributed to the reduction of the local electron density in the surface region and the generation of electric fields (particularly in larger particles) in the SCL that aid the spatial separation of charges. This effect is likely to be critical to the high photocurrent densities reported for hematite photoanodes.

We turn now to the effect of applied bias on the transient signal at 575 nm. Figure 2D demonstrates that anodic bias accelerates this signal decay (in contrast to the retardation at 750 nm) and causes its inversion to a negative (bleach) signal at long times. We have previously assigned this bleach to electron trapping/relaxation into localized states close to the conduction band edge[22] (see Figure 3). Under flat-band conditions, these states are fully occupied (reduced); no bleaching signal is observed at any time delay (ps−s). However, under anodic bias these states can become unoccupied (oxidized) within the SCL, enabling ground state absorption into these states (we note it is
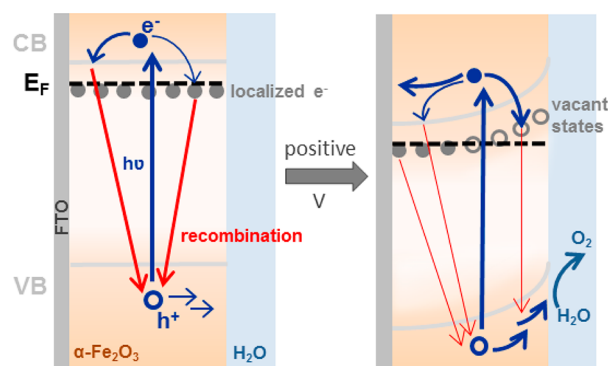

Figure 3. Schematic indicating effect of applied positive bias on hematite: the surface becomes depleted of electrons, resulting in band bending in larger particles (for simplicity the illustration neglects possible effects of Fermi level pinning). This band bending aids spatial separation of the charges. In addition, localized states vacated by this electron depletion (empty circles in figure) can trap photogenerated electrons, further retarding recombination and thus facilitating hole transport to the photoanode surface.

likely that some Fermi level pinning occurs). Following photoexcitation, relaxation of photogenerated electrons into these unoccupied states (i.e., electron trapping) can result in bleaching (loss) of the ground state absorption. This leads to a negative transient absorption, as observed at 575 nm under anodic bias (Figure 2). As the anodic bias is increased, the intensity (depth) of the bleach signal increases, consistent with electron trapping into unoccupied states within the SCL. Importantly, Figure 2 indicates that this electron trapping process is initiated on subpicosecond time scales and thus may compete with electron/hole recombination, discussed further below. The bleaching signal recovers on the 1−10 ms time scale, assigned previously to extraction of these trapped electrons to the external circuit, in kinetic competition with recombination with photogenerated holes.[2]

The electron trapping process described above is likely to be distinct from initial hot electron relaxation to the conduction band edge, which has been reported to occur in hematite on faster time scales (τ 240 fs; <300 fs).[10,23] We note that, for some hematite films, a partial inversion of the 575 nm absorption peak is observed even in the absence of anodic bias, assigned to SCL formation at the semiconductor/liquid junction. Consequently, faster decay kinetics are observed around 575 nm than in other spectral regions (Figure S8). This may in part explain some reports of extremely fast "recombination" kinetics, where the transient signal apparently decays to zero within hundreds of picoseconds.

The ps−μs electron/hole recombination reported herein is the primary process limiting the transfer to, and accumulation of, long-lived holes at the electrode surface, which is required for water oxidation on hematite[2] ($\sim$1 s decay phase in Figure 2E under anodic bias). This transfer is likely to be limited by the low mobility of holes in hematite.[24] Ultrafast electron trapping/localization (as monitored at 575 nm) could significantly reduce electron/hole recombination losses during this hole transfer process. Subsequently, thermally activated recombination of these trapped electrons with surface holes may be mitigated by the band bending in the SCL,[7] thus enabling more efficient extraction of electrons to the external circuit. This requirement to retard ultrafast electron/hole recombination by SCL formation is likely to be one of the

reasons for the rather large overpotentials required for photocurrent generation by hematite. The lower overpotentials typically required for TiO$_2$ are consistent with its slower recombination kinetics (as well as its faster water oxidation kinetics),[25] although several other factors may also contribute to the overpotential.

The results reported herein indicate that electron trapping in hematite occurs on the same time scale as ultrafast electron/hole recombination, and may therefore aid the generation of long-lived charge carriers. These localized/trap states close to the conduction band edge may be associated with dopants, oxygen vacancies[22] and/or Fe^{II} small polarons,[23] thus might also be involved in electron transport. Theoretical studies of hematite have suggested that electrons trapped on oxygen vacancies cannot immediately recombine.[26] We note that doping of hematite (such as Si doping for the photoanodes studied herein) may increase the density of such localized states within the SCL, providing an additional mechanism for the significant increases in water oxidation efficiency observed upon doping.[27,28] These states are likely to be distinct from those due to surface adsorbates.[29]

There have been many previous reports of ultrafast charge carrier recombination in metal oxide photoelectrodes. However, studies under applied bias conditions employed in photoelectrochemical cells, and studies relating ultrafast recombination to photoelectrochemical function, have been very limited to date. It is apparent from the data reported herein that hematite exhibits recombination 100−1000 times faster than anatase TiO$_2$ measured under comparable conditions. We show that anodic bias can significantly retard this ultrafast electron/hole recombination in hematite, attributed primarily to space charge layer formation. Our results indicate that electron trapping into localized states within the SCL of hematite may compete with electron/hole recombination, facilitating efficient hole transfer to the hematite surface. This requirement to retard ultrafast electron/hole recombination by SLC formation, and consequent electron localization, is likely to be one of the reasons for the significant overpotentials required for photocurrent generation by hematite photoanodes for water oxidation.

ASSOCIATED CONTENT

S **Supporting Information**

Experimental details; photogenerated carrier concentrations and SCL width estimations; additional TAS data; UV−vis spectra; i/V curves. This material is available free of charge via the Internet at http://pubs.acs.org.

AUTHOR INFORMATION

Corresponding Authors
s.pendlebury@imperial.ac.uk
j.durrant@imperial.ac.uk

Notes

The authors declare no competing financial interest.

ACKNOWLEDGMENTS

REFERENCES

(1) Cowan, A. J.; Tang, J. W.; Leng, W. H.; Durrant, J. R.; Klug, D. R. J. Phys. Chem. C **2010**, 114, 4208.
(2) Pendlebury, S. R.; Cowan, A. J.; Barroso, M.; Sivula, K.; Ye, J.; Grätzel, M.; Klug, D. R.; Tang, J.; Durrant, J. R. Energy Environ. Sci. **2012**, 5, 6304.
(3) Peter, L. M.; Wijayantha, K. G. U.; Tahir, A. A. Faraday Discuss. **2012**, 155, 309.
(4) Ma, Y.; Pendlebury, S. R.; Reynal, A.; Le Formal, F.; Durrant, J. R. Chem. Sci. **2014**, DOI: 10.1039/C4SC00469H.
(5) Yamanaka, K.-i.; Morikawa, T. J. Phys. Chem. C **2012**, 116, 1286.
(6) Huang, Z.; Lin, Y.; Xiang, X.; Rodríguez-Córdoba, W.; McDonald, K. J.; Hagen, K. S.; Choi, K.-S.; Brunschwig, B. S.; Musaev, D. G.; Hill, C. L.; Wang, D.; Lian, T. Energy Environ. Sci. **2012**, 5, 8923.
(7) Le Formal, F.; Pendlebury, S. R.; Cornuz, M.; Tilley, S. D.; Grätzel, M.; Durrant, J. R. J. Am. Chem. Soc. **2014**, 136, 2564.
(8) Cherepy, N. J.; Liston, D. B.; Lovejoy, J. A.; Deng, H.; Zhang, J. Z. J. Phys. Chem. B **1998**, 102, 770.
(9) Nadtochenko, V. A.; Denisov, N. N.; Gak, V. Y.; Gostev, F. E.; Titov, A. A.; Sarkisov, O. M.; Nikandrov, V. V. Russ. Chem. Bull. **2002**, 51, 457.
(10) Joly, A. G.; Williams, J. R.; Chambers, S. A.; Xiong, G.; Hess, W. P.; Laman, D. M. J. Appl. Phys. **2006**, 99, 053521.
(11) Ling, Y.; Wang, G.; Wheeler, D. A.; Zhang, J. Z.; Li, Y. Nano Lett. **2011**, 11, 2119.
(12) Shen, S.; Guo, P.; Wheeler, D. A.; Jiang, J.; Lindley, S. A.; Kronawitter, C. X.; Zhang, J. Z.; Guo, L.; Mao, S. S. Nanoscale **2013**, 5, 9867.
(13) Fitzmorris, B. C.; Patete, J. M.; Smith, J.; Mascorro, X.; Adams, S.; Wong, S. S.; Zhang, J. Z. ChemSusChem **2013**, 6, 1907.
(14) Kim, J. Y.; Magesh, G.; Youn, D. H.; Jang, J. W.; Kubota, J.; Domen, K.; Lee, J. S. Sci. Rep **2013**, 3, 2681.
(15) Zhong, D. K.; Cornuz, M.; Sivula, K.; Gratzel, M.; Gamelin, D. R. Energy Environ. Sci. **2011**, 4, 1759.
(16) Tilley, S. D.; Cornuz, M.; Sivula, K.; Gratzel, M. Angew. Chem., Int. Ed. **2010**, 49, 6405.
(17) Gimeno, N.; Li, X.; Durrant, J. R.; Vilar, R. Chem.—Eur. J. **2008**, 14, 3006.
(18) Gilbert, B.; Katz, J. E.; Huse, N.; Zhang, X.; Frandsen, C.; Falcone, R. W.; Waychunas, G. A. Phys. Chem. Chem. Phys. **2013**, 15, 17303.
(19) Furube, A.; Asahi, T.; Masuhara, H.; Yamashita, H.; Anpo, M. J. Phys. Chem. B **1999**, 103, 3120.
(20) Nelson, J.; Chandler, R. E. Coord. Chem. Rev. **2004**, 248, 1181.
(21) Cesar, I.; Sivula, K.; Kay, A.; Zboril, R.; Gratzel, M. J. Phys. Chem. C **2009**, 113, 772.
(22) Barroso, M.; Pendlebury, S. R.; Cowan, A. J.; Durrant, J. R. Chem. Sci. **2013**, 4, 2724.
(23) Vura-Weis, J.; Jiang, C.-M.; Liu, C.; Gao, H.; Lucas, J. M.; de Groot, F. M. F.; Yang, P.; Alivisatos, A. P.; Leone, S. R. J. Phys. Chem. Lett. **2013**, 4, 3667.
(24) Gardner, R. F. G.; Moss, R. L.; Tanner, D. W. Br. J. Appl. Phys. **1966**, 77, 55.
(25) Cowan, A. J.; Barnett, C. J.; Pendlebury, S. R.; Barroso, M.; Sivula, K.; Graetzel, M.; Durrant, J. R.; Klug, D. R. J. Am. Chem. Soc. **2011**, 133, 10134.
(26) Rivera, R.; González, S.; Stashans, A. Superlatt. Microstruct. **2010**, 47, 225.
(27) Ling, Y.; Wang, G.; Reddy, J.; Wang, C.; Zhang, J. Z.; Li, Y. Angew. Chem., Int. Ed. **2012**, 51, 4074.
(28) Yang, T. Y.; Kang, H. Y.; Sim, U.; Lee, Y. J.; Lee, J. H.; Koo, B.; Nam, K. T.; Joo, Y. C. Phys. Chem. Chem. Phys. **2013**, 15, 2117.
(29) Du, C.; Zhang, M.; Jang, J.-W.; Liu, Y.; Liu, G.-Y.; Wang, D. J. Phys. Chem. C **2014**, DOI: 10.1021/jp5006346.